Environmental Pollution 264 (2020) 114691

Contents lists available at ScienceDirect

Environmental Pollution

journal homepage: www.elsevier.com/locate/envpol

Improvement in hourly $PM_{2.5}$ estimations for the Beijing-Tianjin-Hebei region by introducing an aerosol modeling product from MASINGAR☆

Yixiao Zhang [a], Wei Wang [a, *], Yingying Ma [b], Lixin Wu [a], Weiwei Xu [a], Jia Li [a]

[a] School of Geosciences and Info-Physics, Central South University, Changsha, 410083, China
[b] State Key Laboratory of Information Engineering in Surveying, Mapping and Remote Sensing, Wuhan University, Wuhan, 430079, China

ARTICLE INFO

Article history:
Received 29 January 2020
Received in revised form
16 April 2020
Accepted 27 April 2020
Available online 29 April 2020

Keywords:
$PM_{2.5}$
Himawari-8
Remote sensing
Linear mixed effects
Geographically weighted regression

ABSTRACT

This study improves traditional $PM_{2.5}$ estimation models by combining an hourly aerosol optical depth from the Advanced Himawari Imager onboard Himawari-8 with a newly introduced predictor to estimate hourly $PM_{2.5}$ concentrations in the Beijing–Tianjin–Hebei (BTH) region from November 1, 2018 to October 31, 2019. The new predictor is an hourly $PM_{2.5}$ forecasting product from the Model of Aerosol Species IN the Global AtmospheRe (MASINGAR). Comparative experiments were conducted by utilizing three extensively used regression models, namely, multiple linear regression (MLR), geographically weighted regression (GWR), and linear mixed effects (LME). A ten-fold cross validation (CV) demonstrated that the MASINGAR product significantly improved the performances of these models. The introduced product increased the model's determination coefficients (from 0.316 to 0.379 for MLR, from 0.393 to 0.445 for GWR, and from 0.718 to 0.765 for LME), decreased their root mean square errors (from 38.2 $\mu g/m^3$ to 36.4 $\mu g/m^3$ for MLR, from 36.0 $\mu g/m^3$ to 34.4 $\mu g/m^3$ for GWR, and from 24.5 $\mu g/m^3$ to 22.4 $\mu g/m^3$ for LME) and mean absolute errors (from 25.2 $\mu g/m^3$ to 23.3 $\mu g/m^3$ for MLR, from 23.5 $\mu g/m^3$ to 21.8 $\mu g/m^3$ for GWR, and from 15.2 $\mu g/m^3$ to 13.7 $\mu g/m^3$ for LME). Then, a well-trained LME model was utilized to estimate the spatial distributions of hourly $PM_{2.5}$ concentrations. Highly polluted localities were clustered in the central and southern areas of the BTH region, and the least polluted area was in northwestern Hebei. Seasonal $PM_{2.5}$ levels averaged from the hourly estimations exhibited the highest concentrations (55.4 ± 56.8 $\mu g/m^3$) in the winter and lowest concentrations (25.1 ± 18.2 $\mu g/m^3$) in the summer.

Main finding: Introducing the $PM_{2.5}$ products from MASINGAR can significantly improve the performance of traditional models for surface $PM_{2.5}$ estimations by 7–20%.

1. Introduction

Rapid industrialization and urbanization in China in this century have led to severe industrial aerial contamination and massive amounts of atmospheric fine particulate matter ($PM_{2.5}$, i.e., particulates less than 2.5 μm in diameter) (Zhang and Cao, 2015). The global atmospheric environment has received much attention because of repeated air pollution incidents that have considerably affected human health (Anderson et al., 2012). Poisonous substances constitute $PM_{2.5}$, which are then inhaled by humans and transported directly into the bronchi, affecting gas exchange in the lungs, damaging respiratory and cardiovascular systems, and inducing asthma, bronchitis, and cardiovascular diseases (Huang et al., 2011; Zhang et al., 2019). High $PM_{2.5}$ levels considerably decrease atmospheric visibility and influence daily traffic forward (Cheung et al., 2005; Yang et al., 2007). As the main component of aerosols, $PM_{2.5}$ affects climate systems both directly and indirectly (Feng and Zou, 2019, 2020; Jonsson et al., 2004). The spatiotemporal distribution of $PM_{2.5}$ loadings must therefore be monitored and predicted to safeguard public health and prevent environmental pollution.

Large quantities of pollution data should be obtained to heighten particle level control, considering that $PM_{2.5}$ is strongly associated with human health and the environment (Zhang et al.,

☆ This paper has been recommended for acceptance by Pavlos Kassomenos

* Corresponding author.
E-mail address: wangweicn@csu.edu.cn (W. Wang).

https://doi.org/10.1016/j.envpol.2020.114691
0269-7491/

2019). Ground-based measurement is the primary technique for traditional environmental monitoring; this technique has advanced $PM_{2.5}$ estimation accuracy and reliability, but punctuated field observations cannot be applied in regional range calculations (Wang et al., 2019b; Zhang et al., 2016). Monitoring stations in China are sporadically distributed and exhibit low spatial continuity (Wang et al., 2019b). Lidar can obtain vertical particulate matter (Raut and Chazette, 2009), aerosol properties (Li et al., 2016; Mao et al., 2012), chlorophyll (Yang et al., 2019a; Yang et al., 2019b) and so on, but it is also difficult to observe pollution level over a large-scale region. Satellite-based monitoring data from a passive sensor, which have a wide distribution range, can compensate for ground measurement limitations (Du et al., 2014; Hong et al., 2020; Li et al., 2012). Aerosol optical depth (AOD) is a critical correlative parameter of ground $PM_{2.5}$ loadings that can extrapolate site-based $PM_{2.5}$ measurements to a regional range.

An efficient estimation model for AOD and $PM_{2.5}$ is crucial for obtaining regional $PM_{2.5}$ values. Numerous models, such as multiple linear regression (MLR) (Pawan and Christopher, 2009), linear regression (Chu et al., 2003), linear mixed effects (LME) (Ma et al., 2016; Wang et al., 2017), geographically weighted regression (GWR) (Hu et al., 2013; Zhang et al., 2016), and artificial neural network (Pawan et al., 2009; Singh et al., 2012) models, have been utilized to determine the correlation between AOD and $PM_{2.5}$ near the surface. However, improving model performances to satisfy the current requirements of atmospheric pollution monitoring and research remains a challenge.

Numerous studies (Chen et al., 2014; Guo et al., 2014; Paciorek and Liu, 2012; Song et al., 2014) have indicated that, except for the application of linear and nonlinear models, the fitting effect of AOD−$PM_{2.5}$ can be improved by adding meteorological parameters, aerosol vertical distribution characteristics, and underlying surface information to the AOD−$PM_{2.5}$ correlation model. The air temperature (TEMP), wind speed (WS), relative humidity (RH), precipitation (PREC), normalized difference vegetation index (NDVI), boundary layer height (BLH), and digital elevation model (DEM) are used as predictors in the widely adopted models (Jing et al., 2015; Ni et al., 2017; Zheng et al., 2015). However, the performances of these models are limited by the undefined relationship between the aforementioned factors and ground $PM_{2.5}$ concentrations. A new predictor, namely, the hourly forecast $PM_{2.5}$ product from the Model of Aerosol Species IN the Global AtmospheRe (MASINGAR), was introduced in this study to improve these models.

The remainder of this paper is divided into several sections. Sections 2 and 3 describe the study region and satellite-based models that estimate hourly $PM_{2.5}$ pollution levels, respectively. Section 4 presents the estimation and validation of hourly $PM_{2.5}$ concentrations. The spatiotemporal distributions of hourly and seasonal $PM_{2.5}$ concentrations are also demonstrated in this section.

2. Study region and datasets

2.1. Study region

The Chinese government aims to enhance the air quality in China and has therefore initiated nationwide air quality monitoring. This study acquired hourly site-based $PM_{2.5}$ observations from 1581 $PM_{2.5}$ monitoring sites operated by the China National Environmental Monitoring Center (CNEMC) (http://www.cnemc.cn/). These monitoring stations are supervised by the China Meteorological Administration, as shown in Fig. 1.

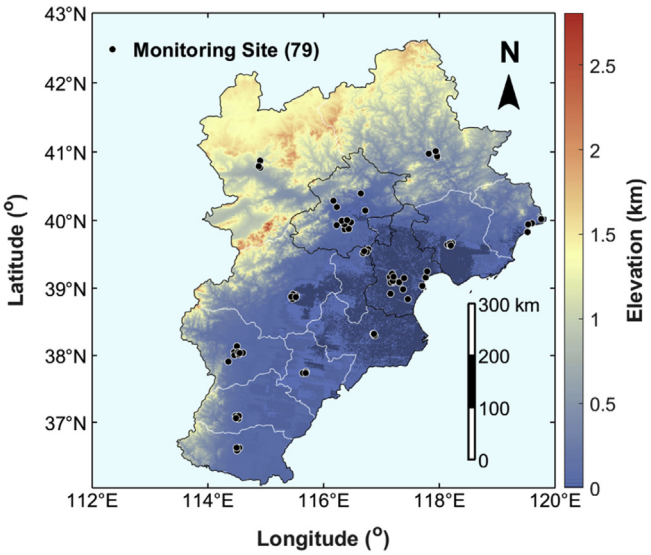

Fig. 1. Spatial distribution of $PM_{2.5}$ monitoring networks supervised by the CNEMC.

2.2. Datasets

Advanced Himawari Imager (AHI) AOD and relevant auxiliary data with $PM_{2.5}$ loading evolutions, including meteorological, geological, and topographic factors, constituted the datasets used in this study. The period covered by the datasets was November 1, 2018 to October 31, 2019. Table 1 presents the details of the datasets.

Himawari-8 is a geostationary weather satellite that covers the region from 80° E to 160° W and from 60° N to 60° S (Kurihara et al., 2016). Its primary AHI sensor can retrieve aerosol optical properties at 500 nm with a 5-km spatial resolution (Wang et al., 2019a; Yumimoto et al., 2016). This study applied AHI hourly AOD (level 3, version 3) with the highest confidence level ("very good").

(2) MASINGAR PM2.5 (MAPM) product

The introduced MAPM product forecasts hourly aerosol properties using the Meteorological Research Institute (MRI)/Japan Meteorological Agency global aerosol model (MASINGAR). This product is assimilated by Himawari L3 AOD at 00:00, 03:00, 06:00, and 09:00 UTC (Yumimoto et al., 2018). The opposite side of the Himawari observation area is updated at 12:00 and 18:00 UTC using Moderate Resolution Imaging Spectroradiometer (MODIS)/(Terra + Aqua) L3 AOD. The products were produced by the Meteorological Research Institute and were provided by the Japan Aerospace Exploration Agency P-Tree System. The MASINGAR $PM_{2.5}$ product at ground level was used in this study.

(3) Meteorological data

This study considered meteorological factors derived from the ERA5 reanalysis dataset. The European Center for Medium-Range Weather Forecasts established the ERA5 as their fifth-generation climate reanalysis dataset (Urraca et al., 2018). Unlike ERA-Interim, ERA5 has a finer spatial grid (31 km versus 79 km), greater time resolution (1 h versus 3 h), more vertical levels (137 versus 60 levels), a new numerical weather prediction model (i.e., IFS Cycle 41r2), and additional assimilated data. Table 1 shows the surface meteorological factors utilized in this study, namely, TEMP, RH, PREC, WS, and BLH.

Table 1
Summary of datasets used in this study.
(1) Himawari-8/AHI-measured aerosol products

Data	Variable	Unit	Temporal resolution	Spatial Resolution	Source
$PM_{2.5}$	$PM_{2.5}$	$\mu g/m^3$	1 h	Site	CNEMC
AOD	AOD	Unitless	1 h	5 km	AHI
Forecasted $PM_{2.5}$	$PM_{2.5}$	$\mu g/m^3$	1 h	~0.375°	MASINGAR
Meteorological factors	RH	%	1 h	0.25°	ERA5
	TEMP	K	1 h	0.25°	
	WS	m/s	1 h	0.25°	
	BLH	m	1 h	0.25°	
Geological factor	NDVI	Unitless	16 d	0.05°	MODIS
Topographic factor	DEM	m	–	90 m	USGS

(4) Land type data

The NDVI was utilized as a proxy for surface type. The data were derived from MODIS 16-day NDVI products, namely, "CMG 0.05 Deg 16 days NDVI" in "MOD13C1/MYD13C1". Vegetated areas typically exhibit a high NDVI, whereas a surface dominated by soil generally exhibits a low NDVI.

(5) Geographic data

The DEM (with a spatial resolution of 90 m) was obtained from the Consortium for Spatial Information of the United States Geological Survey (USGS) (http://srtm.csi.cgiar.org/srtmdata/). The DEM was interpolated to the same spatial resolution as the AHI AOD (5 km) in this study.

3. Methodology

3.1. Estimation models

MLR, GWR, and LME, which are extensively used regression models, were utilized in this study, and their performance was compared based on different predictors.

(1) MLR

The MLR model (Gupta and Christopher, 2009) is expressed as

$$PM_{2.5} = b + a_1 \times AOD + a_2 \times TEMP + a_3 \times RH + a_4 \times WS + a_5 \times PREC + a_6 \times NDVI + a_7 \times BLH + a_8 \times TF + \varepsilon, \quad (1)$$

where $a_1, \ldots, a_n$ are regression coefficients, b indicates the intercept, and ε denotes the error term. The iMLR model is the MLR model with MAPM introduced as a new predictor. The iMLR model is expressed as

$$PM_{2.5} = b + a_1 \times AOD + a_9 \times MAPM + a_2 \times TEMP + a_3 \times RH + a_4 \times WS + a_5 \times PREC + a_6 \times NDVI + a_7 \times BLH + a_8 \times TF + \varepsilon, \quad (2)$$

where a_9 is the regression coefficient for MAPM.

(2) GWR

The GWR model (Hu et al., 2013; Zhang et al., 2016) is presented as

$$PM_{2.5s} = b_0(i,j) + b_1(i,j) \times AOD_s + b_2(i,j) \times TEMP_s + b_3(i,j) \times RH_s + b_4(i,j) \times WS_s + b_5(i,j) \times PREC_s + b_6(i,j) \times NDVI_s + b_7(i,j) \times BLH_s + b_8(i,j) \times TF_s + \varepsilon_s, \quad (3)$$

where $PM_{2.5s}$ denotes the $PM_{2.5}$ loading at location $s(i, j)$, b_0 refers to the intercept, b_1 and b_n are slopes for different predictors, and ε_s is the error term. The iGWR model is the GWR model with MAPM introduced as a new predictor. The iGWR model is expressed as

$$PM_{2.5s} = b_0(i,j) + b_1(i,j) \times AOD_s + b_9(i,j) \times MAPM_s + b_2(i,j) \times TEMP_s + b_3(i,j) \times RH_s + b_4(i,j) \times WS_s + b_5(i,j) \times PREC_s + b_6(i,j) \times NDVI_s + b_7(i,j) \times BLH_s + b_8(i,j) \times TF_s + \varepsilon_s, \quad (4)$$

where a_9 is the slope for MAPM. The distance weights were derived by a universal gaussian kernel function in the GWR and iGWR models.

(3) LME

The LME model extends the ordinary linear regression model and is used to estimate $PM_{2.5}$ because its time-specific random effect can interpret the temporal variation correlations between $PM_{2.5}$ and different predictors in a particular area (Wang et al., 2017; Wang et al., 2019b). The LME model is expressed as

$$PM_{.2.5_{n,m}} = \left[\beta_0 + b^{day}_{0,n,m}\right] + \left[\beta_1 + b^{day}_{1,n,m}\right] \times AOD_{n,m} + \beta_2 \times TEMP_{n,m} + \beta_3 \times RH_{n,m} + \beta_4 \times WS_{n,m} + \beta_5 \times PREC_{n,m} + \beta_6 \times NDVI_{n,m} + \beta_7 \times BLH_{n,m} + \beta_8 \times TF_{n,m} + \varepsilon_{n,m}, \left(b^{day}_{0,n,m}, b^{day}_{1,n,m}\right) \sim N\left[\left(0,0,\sum\right)\right], \varepsilon_{n,m} \sim N\left(0,\sigma^2\right), \quad (5)$$

where n is the grid index; m indicates the time; β_0 and $\beta_1-\beta_8$represent the fixed intercept and random slopes of the corresponding predictors, respectively; $b_{0,n,m}^{day}$ and $b_{1,n,m}^{day}$ indicate the time-specific random intercept and random slope of the AOD predictor, respectively; $\varepsilon_{n,m} \sim N(0,\sigma^2)$ indicates the error term; and $\sum$ represents the variance−covariance matrix of the random effects. The iLME model is the LME model with MAPM introduced as a new predictor. The model can be expressed as

$$PM_{.2.5_{n,m}} = \left[\beta_0 + b_{0,n,m}^{day}\right] + \left[\beta_1 + b_{1,n,m}^{day}\right] \times AOD_{n,m} + \left[\beta_9 + b_{9,n,m}^{day}\right] \times MAPM_{n,m} + \beta_2 \times TEMP_{n,m} + \beta_3 \times RH_{n,m} + \beta_4 \times WS_{n,m} + \beta_5 \times PREC_{n,m} + \beta_6 \times NDVI_{n,m} + \beta_7 \times BLH_{n,m} + \beta_8 \times TF_{n,m} + \varepsilon_{n,m}, \left(b_{0,n,m}^{day}, b_{1,n,m}^{day}\right) \sim N\left[\left(0,0,\sum\right)\right], \varepsilon_{n,m} \sim N\left(0,\sigma^2\right), \quad (6)$$

where β_9 and $b_9$represent fixed and random slopes of MAPM, respectively.

3.2. Spatiotemporal matching

This study reprocessed all used data for spatial and temporal consistency, and a matched dataset was formed as the fundamental sample to train different models. The satellite-based AOD, meteorologically forecasted $PM_{2.5}$, and geographic factors, which have different spatial resolutions, were interpolated to the same spatial resolution and scope as those of the AHI AOD (5 km). Two criteria were used to derive the factors around the PM-monitoring sites. First, the matching spatial distance should be within a 5-km radius from the site center. Second, the matching time difference should be within 1 h of the AHI measuring time. Moreover, the hourly average measurements of surface $PM_{2.5}$ were correlated with the values of satellite AODs and meteorological and geographic factors in the study area.

3.3. Evaluation approaches

The performances of these models in estimating $PM_{2.5}$ concentrations were evaluated by conducting 10-fold CVs. The models were trained using 90% of the samples, and the trained models were evaluated using the remaining 10% of the samples. All samples were tested after repeating this process 10 times and testing a different sample set for each iteration. The $PM_{2.5}$ concentrations estimated by the 10-fold CV method were contrasted with those of the site-based observations. The determination coefficient (R^2), root mean square error (RMSE), and mean absolute error (MAE) were used as indicators to evaluate the performances of different models.

4. Results and discussion

4.1. Performance of the MAPM product

The performance of the MAPM at different times (09:00 to 16:00 local times) was assessed and analyzed by performing a contrastive experiment between forecasted $PM_{2.5}$ levels from MASINGAR and ground measurements using a series of quantitative statistical indicators including the correlation coefficient (R), RMSE, and MAE. As shown in Fig. 2(a), MAPM exhibited a poor performance with an overall low R (0.44), high RMSE (49.3 μg/m^3), and high MAE (26.4 μg/m^3). The hourly assessment result varied minimally as shown in Fig. 2(b)–(i). The R value was between 0.42 and 0.49, RMSE was between 42.8 μg/m^3 and 53.5 μg/m^3, and MAE was between 22.1 μg/m^3 and 30.7 μg/m^3. The MAPM performed best at 16:00 LT. In short, the forecasted hourly $PM_{2.5}$ concentrations from the MASINGAR aerosol product do not meet the requirements for environmental pollution studies due to MAPM poor performance in terms of the three quantitatively statistical indicators. MAPM is only assimilated by aerosol retrievals from Himawari/AHI and MODIS/(Terra + Aqua) (Yumimoto et al., 2018). Therefore, the poor performance of MAPM may be attributed to surface $PM_{2.5}$ measurements has not been integrated in this product. On the other hand, MAPM has a more explicit relationship with ground $PM_{2.5}$ concentrations than that of the widely used meteorological, geological, and topographic factors utilized in traditional models. Therefore, MAPM can improve the performance of widely used models when used in combination with other traditional predictors.

4.2. Improvement in estimation models

MLR, GWR, and LME, which are extensively used regional $PM_{2.5}$ estimation models, were adopted to investigate whether MAPM can be introduced as a new auxiliary predictor to improve their accuracy. The models marked with iMLR, iGWR, and iLME are the traditional MLR, GWR, and LME models with MAPM introduced as a new predictor. The performances of these models were evaluated based on R^2, RMSE, and MAE.

The performance of the three models is depicted in Fig. 3. The traditional MLR model without the MASINGAR product exhibited the worst performance of the three models with the lowest R^2 (0.316), highest RMSE (38.2 μg/m^3), and highest MAE (25.2 μg/m^3). A comparison of the MLR and GWR models revealed that the latter exhibited a 6% increase in estimation accuracy compared with the former; The MLR R^2 increased to 0.394, RMSE decreased to 36.0 μg/m^3, and MAE was reduced to 23.5 μg/m^3. However, the performances of GWR model in other studies are better than that in current study, such as the R^2 is 0.60 for Model fitting in Wei et al. (2019). The relatively poor performance of GWR model in this study may be associated with the lowly spatial coverage of AHI aerosol retrievals. The distance weights in the model rely heavily on abundant samples around an estimated point. The traditional LME model without the MASINGAR product demonstrated a considerably high estimation accuracy (i.e., nearly twice the estimation accuracy of the MLR model) with a R^2 of 0.743, RMSE of 23.4 μg/m^3, and MAE of 14.6 μg/m^3. The introduction of the MASINGAR product enhanced the estimation accuracy of the three models to various extents. For example, the R^2, RMSE, and MAE of the LME model increased to 0.792, decreased to 21.1 μg/m^3, and decreased to 13.0 μg/m^3, respectively.

The performance of each model was compared and verified using the 10-fold CV method. The generated results were similar to those in Fig. 3. The best performance was achieved by the LME model, whose R^2, RMSE, and MAE were 0.718, 24.5 μg/m^3, and 15.2 μg/m^3, respectively. After the MASINGAR product was introduced to the models, the LME CV demonstrated an enhanced

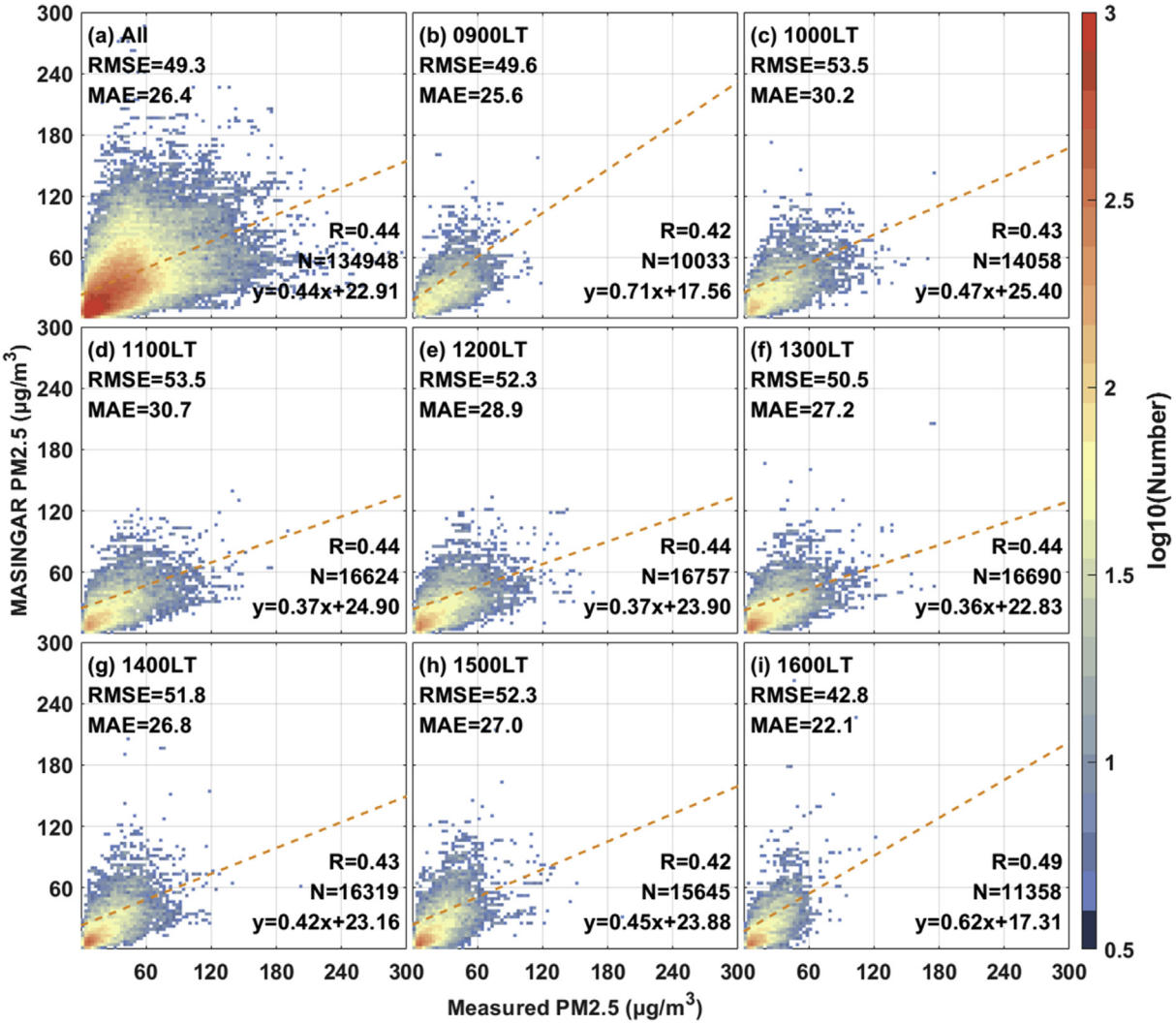

Fig. 2. Scatterplot of forecasted $PM_{2.5}$ levels from MASINGAR aerosol product versus surface $PM_{2.5}$ observations: (a) all obtainable data and (b–i) diurnally diverse hours (09:00 to 16:00 LT).

estimation accuracy. Its R^2 increased to 0.765, RMSE decreased to 22.4 μg/m^3, and MAE decreased to 13.7 μg/m^3, as depicted in Fig. 4.

Given the superior estimation accuracy of the LME model, the LME model was selected as the typical model to demonstrate the improvement in the traditional LME model after introducing MAPM. The temporal variation in surface $PM_{2.5}$ concentration is demonstrated in Fig. 5. The measured $PM_{2.5}$ levels and the estimated results from the LME model with or without the MASINGAR product were compared. Both models exhibited extensive errors from July 2019 to October 2019, but their bias levels differed. The mean absolute bias of the iLME model was 9.4 μg/m^3, whereas that of the original LME model was 10.4 μg/m^3 (9.8% improvement in model performance). The mean total absolute bias of the iLME model was 13.7 μg/m^3, whereas that of the original LME model was 15.2 μg/m^3. The green dotted circle in Fig. 5 indicates that the traditional LME model had negative $PM_{2.5}$ estimations. Moreover, the yellow dotted circle in Fig. 5 demonstrates that the traditional LME model had a large positive deviation in $PM_{2.5}$ estimation compared to that of the iLME model. In summary, these analyses implied that the iLME model demonstrated greater stability and a lower deviation than those of the traditional LME model as a result of the introduced MAPM predictor, which played a significant role in regional $PM_{2.5}$ estimations.

It is worth pointing out that aerosol products from other global chemistry transport models (CTM) (such as GEOS-CHEM, MOZART-4, MERRA, etc.) also has a potential to improve the performance of regional $PM_{2.5}$ estimating models. The reason of MAPM was introduced in this study is that MAPM has a relatively high spatial resolution (~0.375°) than aerosol products from other global CTM. Moreover, MAPM has a same temporal resolution (1 h) with Himawari-8/AHI AOD product.

4.3. Spatial distribution of estimated $PM_{2.5}$ levels

Fig. 6 displays the spatial and hourly distributions of $PM_{2.5}$ levels in the BTH region based on estimations from the iLME model. The total average estimated $PM_{2.5}$ concentration in this region was 38.6 ± 38.6 μg/m^3, which indicates a severe $PM_{2.5}$ pollution level. A significant regional variation was observed; the mean values of estimated $PM_{2.5}$ for different sub-regions were between 13.0 μg/m^3 and 60.8 μg/m^3. The central and southern areas contained highly polluted localities because of the anthropogenic emissions from the rapid urbanization and prosperous economy in these areas. In contrast, northwestern Hebei was the least polluted area.

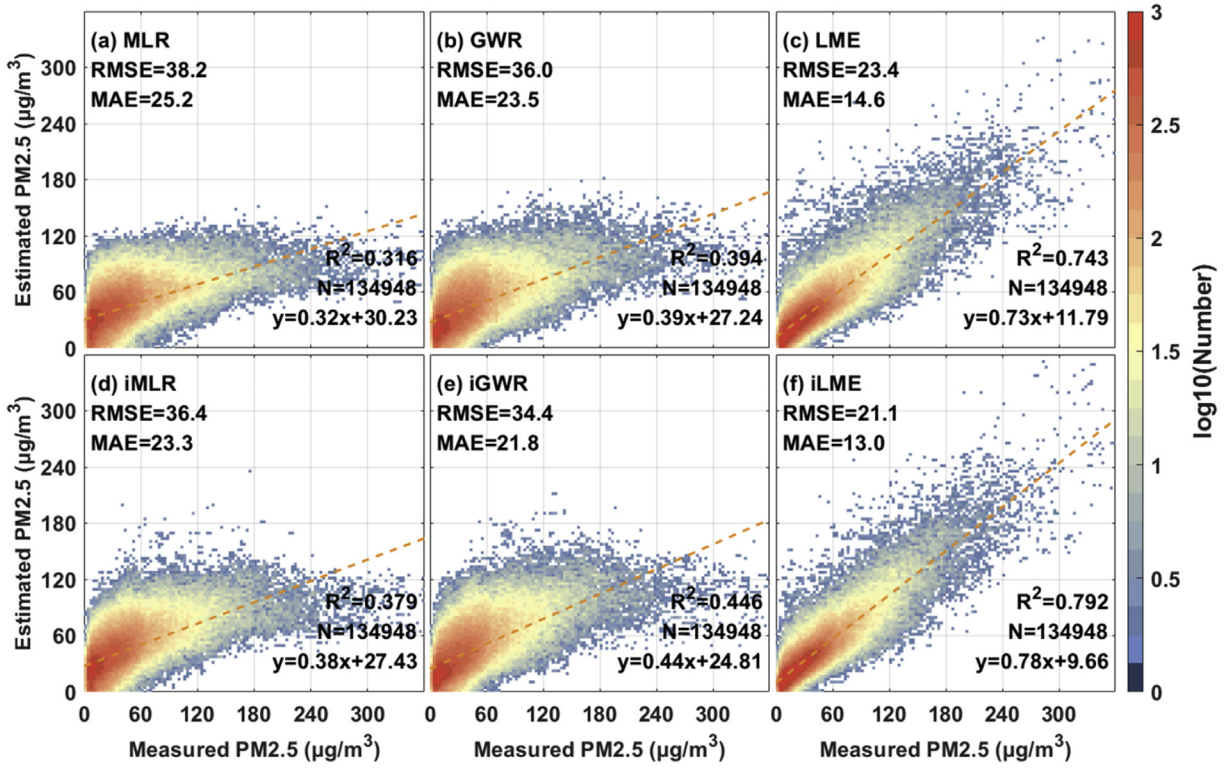

Fig. 3. Scatterplot of measured and estimated $PM_{2.5}$ concentrations (fit) obtained from different models: (a) MLR, (b) GWR, (c) LME, (d) iMLR, (e) iGWR, and (f) iLME. The iMLR, iGWR, and iLME models are MLR, GWR, and LME models with MAPM introduced as a new predictor.

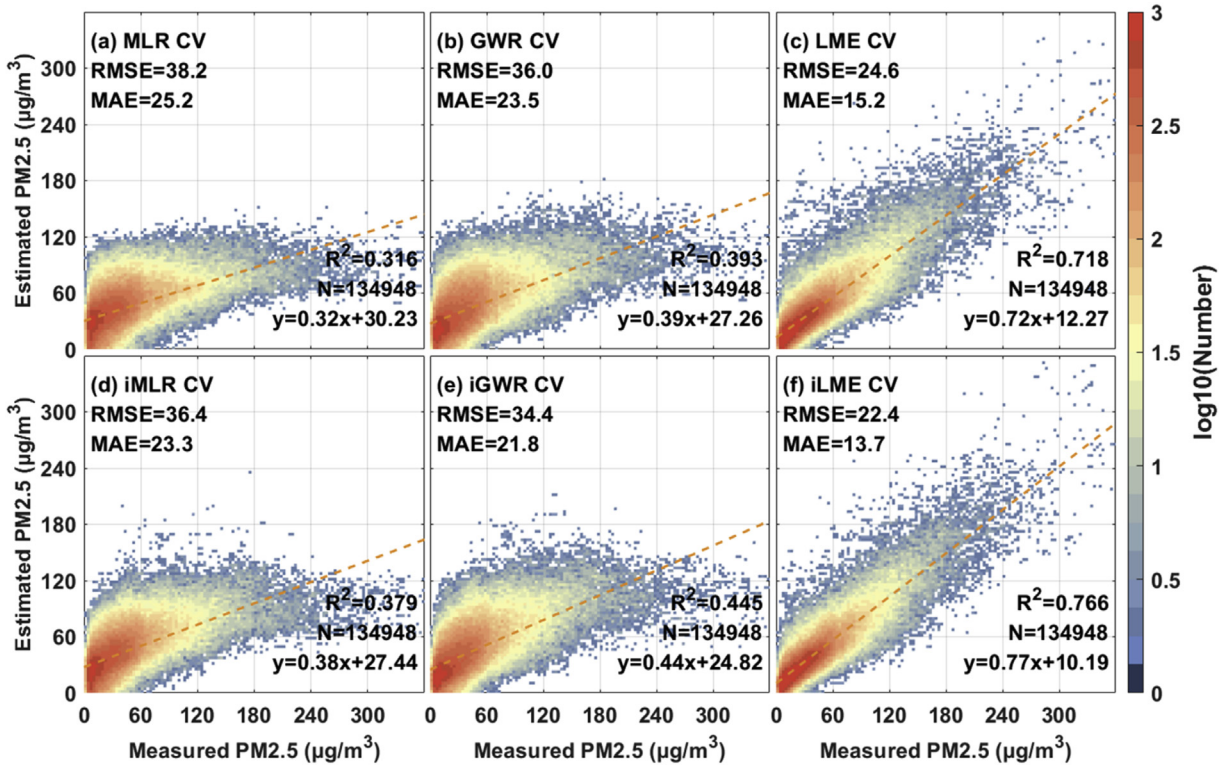

Fig. 4. Scatterplot of measured and estimated $PM_{2.5}$ concentrations obtained from different models: (a) MLR, (b) GWR, (c) LME, (d) iMLR, (e) iGWR, and (f) iLME. The iMLR, iGWR, and iLME models are the MLR, GWR, and LME models with MAPM introduced as a new predictor.

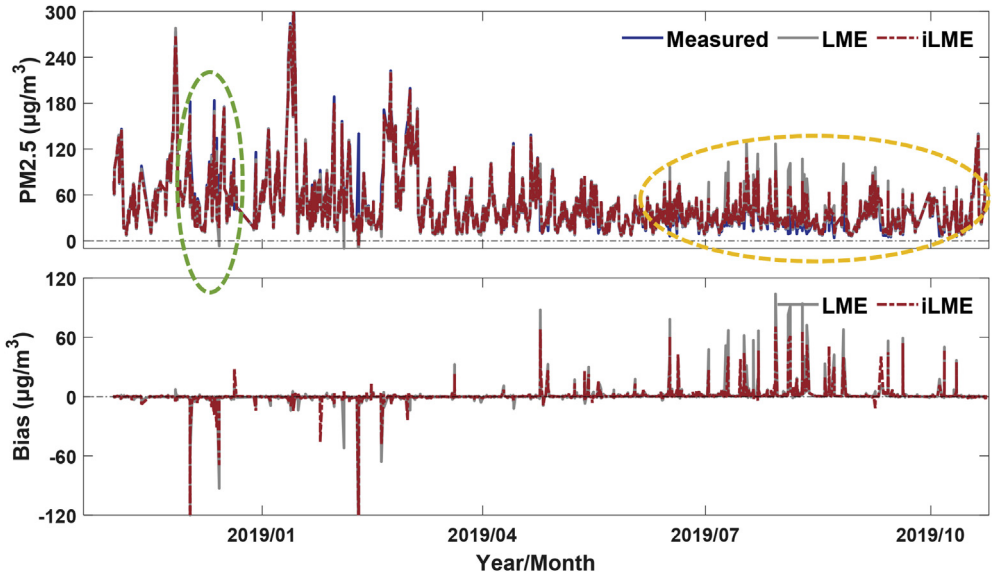

Fig. 5. Variation in estimated $PM_{2.5}$ concentrations from LME and iLME models versus the measured $PM_{2.5}$ and estimation bias contrast between the LME and iLME models within the time frame of this study.

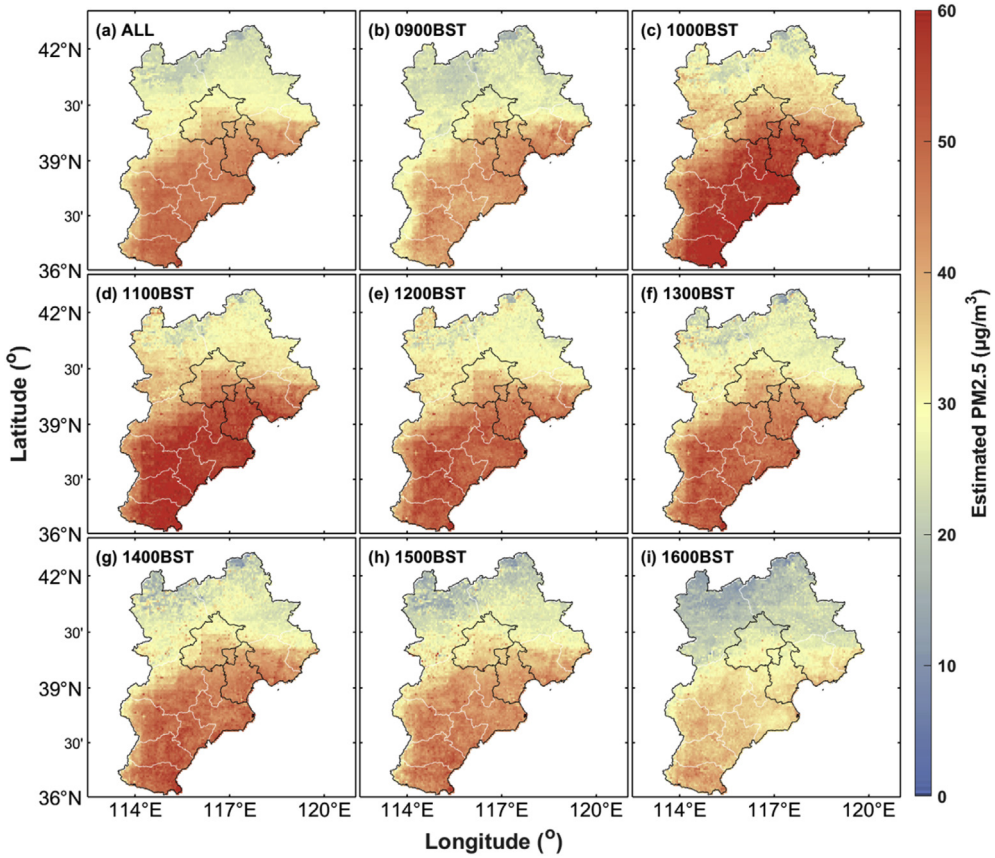

Fig. 6. The spatial distribution of average $PM_{2.5}$ levels attained from the iLME model: (a) all samples and (b–i) diurnally diverse hours (09:00 to 16:00 LT).

Moreover, due to the unfavorable topography of the Taihang Mountains situated in the western Hebei Province, $PM_{2.5}$ pollution in this area may be aggravated because of the topographic limitations and subsequent accumulation of air contaminants in the local regions (Tao et al., 2012).

The daytime $PM_{2.5}$ levels exhibited a distinct variation with the highest value (46.3 ± 39.4 μg/m^3) at 10:00 LT in the BTH region, which was due to rush-hour traffic, and the least-polluted hour was 16:00 LT (lowest $PM_{2.5}$ level of 46.3 ± 39.4 μg/m^3). Moreover, the estimated $PM_{2.5}$ levels displayed a prominent decrease at 14:00 LT when the boundary layer widened. High boundary layers cannot only expand the escape space of surface $PM_{2.5}$ but also facilitate

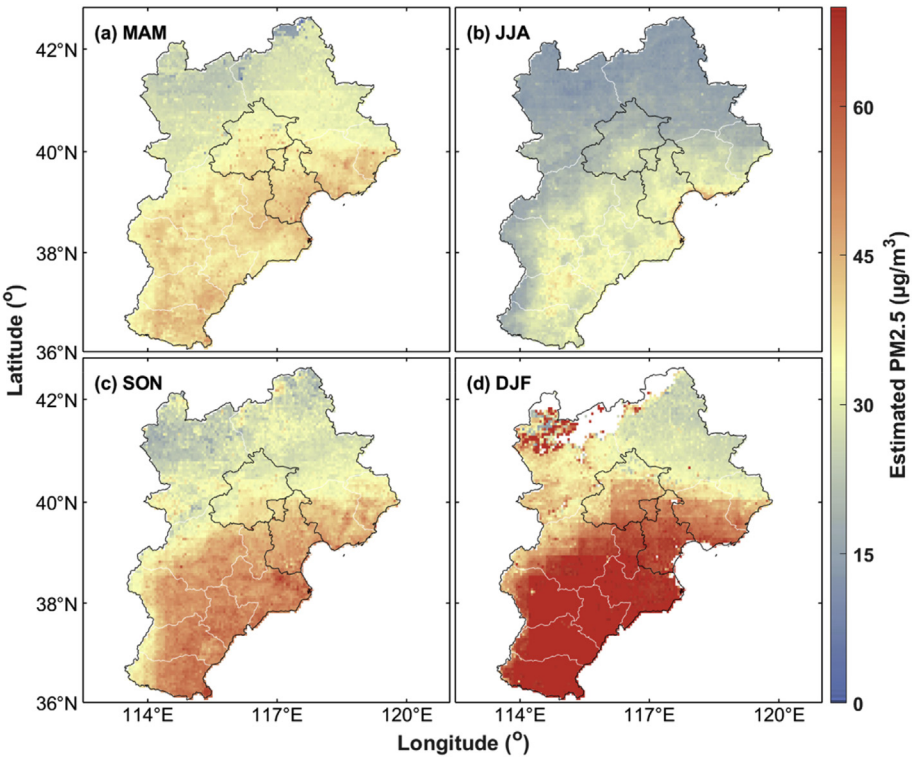

Fig. 7. Spatial distribution of quarterly $PM_{2.5}$ estimations obtained from the iLME model: (a) spring (MAM), (b) summer (JJA), (c) autumn (SON), and (d) Winter (DJF).

vertical convection to dilute pollutants in the atmosphere (Liu et al., 2020; Zhang et al., 2018).

Fig. 7 depicts the spatial and seasonal distributions of $PM_{2.5}$ concentrations. The estimations from the iLME model revealed the remarkable seasonality and regionality of $PM_{2.5}$ concentrations. The most polluted season was winter with a mean estimated $PM_{2.5}$ of 55.4 ± 56.8 μg/m^3, and the least polluted season was summer with an estimated $PM_{2.5}$ of 25.1 ± 18.2 μg/m^3. Moreover, the averagely estimated $PM_{2.5}$ concentration in spring was 36.1 ± 33.5 μg/m^3 and that in summer was 41.4 ± 35.8 μg/m^3. This remarkable seasonal variations are strongly associated with anthropogenic emissions, meteorological condition and so on (Rodriguez et al., 2004; Zhang and Cao, 2015). The maximum wintertime value is further enhanced by the increasing anthropogenic emissions from biomass burning, fossil fuel combustion (Nava et al., 2002; Rushdi et al., 2013) and detrimental meteorological conditions for pollution diffusion (Mao et al., 2020; Noble et al., 2003) (i.e., stagnant weather conditions and temperature inversion during cold periods). The summertime minimum is associated with a reduction in fossil fuel and biomass combustion required for collective heating. The clean air originated from oceans during the East Asian summer monsoon, an intense convection within the atmospheric mixing layer, and the adequate wet depositions of aerosols can also considerably decrease $PM_{2.5}$ concentration (Yoo et al., 2014). Moreover, in this study, seasonality exhibited a lopsided spatial distribution and characteristics that are comparable to those of the diurnal distribution over the BTH region. The spatial distribution of hourly $PM_{2.5}$ concentrations estimated by the LME model demonstrated that the highly polluted localities were clustered in the central and southern areas due to topographic limitations, regional economic factors, and the subsequent accumulation of air pollutants within the area. The least polluted area in the BTH region was northwestern Hebei.

5. Conclusions

This study extensively improved $PM_{2.5}$ estimation models (MLR, GWR, and LME) by introducing a new predictor (i.e., MAPM, an hourly forecast of aerosol properties). The enhanced LME model was used to estimate the spatiotemporal distribution of hourly $PM_{2.5}$ levels in the BTH region. The study period was from November 1, 2018 to October 31, 2019. The following key findings were obtained.

(1) The 10-fold CV results of these widely utilized models indicated that the model performances can be enhanced by the newly introduced MAPM predictor. The traditional LME model exhibited the best performance in $PM_{2.5}$ estimations with the highest R^2 of 0.718, lowest RMSE of 24.5 μg/m^3, and lowest MAE of 15.2 μg/m^3. The introduction of MASINGAR enhanced the LME model capacity for regional $PM_{2.5}$ estimations with an increased R^2 of 0.765, decreased RMSE of 22.4 μg/m^3, and decreased MAE of 13.7 μg/m^3.

(2) The well-trained LME model was used to estimate the spatial distribution of hourly $PM_{2.5}$ concentrations, and significant daily and seasonal variations were observed. The daytime $PM_{2.5}$ exhibited a distinct variation with the highest value (46.3 ± 39.4 μg/m^3) at 10:00 LT in the BTH region. The central and southern BTH regions had high polluted levels, and, in contrast, northwestern Hebei was a low-polluted area.

(3) The seasonal variation in estimated $PM_{2.5}$ loadings revealed a distinct seasonality. The highest concentrations (55.4 ± 56.8 μg/m^3) occurred in winter because of peak combustion emissions. Under the influence of artificial factors and meteorological conditions, summer was the cleanest season with the lowest $PM_{2.5}$ concentrations (25.1 ± 18.2 μg/m^3).

Improving stability and decreasing deviations of these extensively used models by introducing the new MAPM predictor was confirmed in this study. Searching for other predictors that have a clear and direct relationship with surface $PM_{2.5}$ measurements can be explored in future research.

CRediT authorship contribution statement

Yixiao Zhang: Methodology, Validation, Data curation, Writing - original draft. **Wei Wang:** Conceptualization, Methodology, Visualization, Writing - review & editing. **Yingying Ma:** Investigation. **Lixin Wu:** Supervision. **Weiwei Xu:** Methodology. **Jia Li:** Writing - review & editing.

Acknowledgments

This study was supported by the National Key Research and Development Program of China (Grant No. 2018YFC1503600), the National Natural Science Foundation of China (41901295), the leading talents program of Central South University, the Hunan Provincial Talents Gathering Program of China (No. 2018RS3013), the Open Fund of the State Laboratory of Information Engineering in Surveying, Mapping, and Remote Sensing, Wuhan University (Grant No. 18R06), the Innovation Foundation of Shanghai Academy of Spaceflight Technology (No. SAST 2018-042), and the China Postdoctoral Science Foundation (No. 2018M630908). We are also grateful to the China Meteorological Administration, the Data Center of US NASA (https://search.earthdata.nasa.gov/search), the Japan Aerospace Exploration Agency (http://www.eorc.jaxa.jp/ptree), ERA5 (https://cds.climate.copernicus.eu/cdsapp#!/), and USGS (http://srtm.csi.cgiar.org/srtmdata/) for providing the datasets used here.

Appendix A. Supplementary data

Supplementary data to this article can be found online at https://doi.org/10.1016/j.envpol.2020.114691.

Declaration of interests

The authors declare that they have no known competing financial interests or personal relationships that could have appeared to influence the work reported in this paper.

References

Anderson, J.O., Thundiyil, J.G., Stolbach, A., 2012. Clearing the air: a review of the effects of particulate matter air pollution on human health. J. Med. Toxicol. 8, 166–175.
Chen, H., Li, Q., Wang, Z.T., Mao, H.Q., Zhou, C.Y., Zhang, L.J., Chao, X.L., 2014. Study on the methods of monitoring ground-level PM2.5 over Beijing, Tianjin, Hebei region with MODIS data. Journal of Meteorology and Environment 27–37.
Cheung, H.C., Wang, T., Baumann, K., Guo, H., 2005. Influence of regional pollution outflow on the concentrations of fine particulate matter and visibility in the coastal area of southern China. Atmos. Environ. 39, 6463–6474.
Chu, D.A., Kaufman, Y.J., Zibordi, G., Chern, J.D., Holben, H.B., 2003. Global monitoring of air pollution over land from EOS-Terra MODIS. Journal of Geophysical Research Atmospheres 108.
Du, J.W., Tang, T.Y., Huang, M., 2014. Exploring the PM2.5 Pollution Distribution Based on Remote Sensing Image. Electronics World, 187-187.
Feng, H., Zou, B., 2019. Satellite-based estimation of the aerosol forcing contribution to the global land surface temperature in the recent decade. Rem. Sens. Environ. 232, 111299.
Feng, H., Zou, B., 2020. Satellite-based separation of climatic and surface influences on global aerosol change. Int. J. Rem. Sens. 41 (14), 5443–5456.
Guo, Y., Feng, N., Christopher, S.A., Kang, P., Zhan, F.B., Hong, S., 2014. Satellite remote sensing of fine particulate matter (PM2.5) air quality over Beijing using MODIS[J]. Int. J. Rem. Sens. 35, 6522–6544.
Gupta, P., Christopher, S.A., 2009. Particulate matter air quality assessment using integrated surface, satellite, and meteorological products: multiple regression approach. J. Geophys. Res.: Atmosphere 114 (n/a-n/a).
Hong, J., Mao, F., Min, Q., Pan, Z., Wang, W., Zhang, T., Gong, W., 2020. Improved PM2.5 predictions of WRF-Chem via the integration of Himawari-8 satellite data and ground observations. Environ. Pollut. 263, 114451.
Hu, X., Waller, L.A., Al-Hamdan, M.Z., Crosson, W.L., Estes, M.G., Estes, S.M., Quattrochi, D.A., Sarnat, J.A., Liu, Y., 2013. Estimating ground-level PM(2.5) concentrations in the southeastern U.S. using geographically weighted regression. Environ. Res. 121, 1–10.
Huang, Y.C.T., Karoly, E.D., Dailey, L.A., Schmitt, M.T., Silbajoris, R., Graff, D.W., Devlin, R.B., 2011. Comparison of gene expression profiles induced by coarse, fine, and ultrafine particulate matter. J. Toxicol. Environ. Health 74, 296–312.
Jing, R.H., Ma, J.J., Wang, C., 2015. Methods of PM2.5 inversion based on multi-source data[J]. Journal of Atmospheric and Environmental Optics 10.
Jonsson, P., Bennet, C., Eliasson, I., Lindgren, E.S., 2004. Suspended particulate matter and its relations to the urban climate in Dar es Salaam, Tanzania. Atmos. Environ. 38, 4175–4181.
Kurihara, Y., Murakami, H., Kachi, M., 2016. Sea surface temperature from the new Japanese geostationary meteorological Himawari-8 satellite. Geophys. Res. Lett. 43 (n/a-n/a).
Li, J.H., Liu, H.F., Zhao, D.T., 2012. The application progress of AOD retrieval methods based on MODIS [J]. Journal of Green Science and Technology 112–115.
Li, S., Joseph, E., Min, Q., 2016. Remote sensing of ground-level PM2.5 combining AOD and backscattering profile. Rem. Sens. Environ. 183, 120–128.
Liu, B., Ma, Y., Shi, Y., Jin, S., Jin, Y., Gong, W., 2020. The characteristics and sources of the aerosols within the nocturnal residual layer over Wuhan, China. Atmos. Res. 241, 104959.
Ma, Z., Liu, Y., Zhao, Q., Liu, M., Zhou, Y., Bi, J., 2016. Satellite-derived high resolution PM2.5 concentrations in Yangtze River Delta Region of China using improved linear mixed effects model. Atmos. Environ. 133, 156–164.
Mao, F., Gong, W., Ma, Y., 2012. Retrieving the aerosol lidar ratio profile by combining ground-and space-based elastic lidars. Optic Lett. 37, 617–619.
Mao, F., Zang, L., Wang, Z., Pan, Z., Zhu, B., Gong, W., 2020. Dominant synoptic patterns during wintertime and their impacts on aerosol pollution in Central China. Atmos. Res. 232, 104701.
Nava, S., Prati, P., Lucarelli, F., Mandò, P.A., Zucchiatti, A., 2002. Source apportionment in the town of La spezia (Italy) by continuous aerosol sampling and PIXE analysis. Water Air Soil Pollut. Focus 2, 247–260.
Ni, X.Y., Huang, H., Du, W.P., 2017. Relevance analysis and short-term prediction of PM2.5 concentrations in Beijing based on multi-source data. Atmos. Environ. 150, 146–161.
Noble, C.A., Mukerjee, S., Gonzales, M., Rodes, C.E., Lawless, P.A., Natarajan, S., Myers, E.A., Norris, G.A., Smith, L., Oezkaynak, H., 2003. Continuous measurement of fine and ultrafine particulate matter, criteria pollutants and meteorological conditions in urban El Paso, Texas. Atmos. Environ. 37, 827–840.
Paciorek, C.J., Liu, Y., 2012. Assessment and statistical modeling of the relationship between remotely sensed aerosol optical depth and PM2. In: 5 in the Eastern United States, vol. 167, p. 5.
Pawan, Gupta, Sundar, A., Christopher, 2009. Particulate Matter Air Quality Assessment Using Integrated Surface, Satellite, and Meteorological Products: 2. A Neural Network Approach.
Pawan, G., Christopher, S.A., 2009. Particulate matter air quality assessment using integrated surface, satellite, and meteorological products: multiple regression approach. Journal of Geophysical Research Atmospheres 114.
Raut, J.-C., Chazette, P., 2009. Assessment of vertically-resolved PM_{10} from mobile lidar observations. Atmos. Chem. Phys. 9, 8617–8638.
Rodriguez, S., Querol, X., Alastuey, A., Viana, M.-M., Alarcón, M., Mantilla, E., Ruiz, C.R., 2004. Comparative PM10–PM2.5 source contribution study at rural, urban and industrial sites during PM episodes in Eastern Spain. Sci. Total Environ. 328, 95–113.
Rushdi, A.I., Al-Mutlaq, K.F., Al-Otaibi, M., El-Mubarak, A.H., Simoneit, B.R.T., 2013. Air quality and elemental enrichment factors of aerosol particulate matter in Riyadh City, Saudi Arabia. Arabian Journal of Geosciences 6, 585–599.
Singh, K.P., Gupta, S., Kumar, A., Shukla, S.P., 2012. Linear and Nonlinear Modeling Approaches for Urban Air Quality Prediction, vol. 426, 0-0.
Song, W., Jia, H., Huang, J., Zhang, Y., 2014. A satellite-based geographically weighted regression model for regional PM2.5 estimation over the Pearl River Delta region in China[J]. Rem. Sens. Environ. 154, 1–7.
Tao, M., Chen, L., Lin, S., Tao, J., 2012. Satellite observation of regional haze pollution over the North China Plain. Journal of Geophysical Research Atmospheres 117.
Urraca, R., Huld, T., Gracia-Amillo, A., Martinez-de-Pison, F.J., Kaspar, F., Sanz-Garcia, A., 2018. Evaluation of global horizontal irradiance estimates from ERA5 and COSMO-REA6 reanalyses using ground and satellite-based data. Sol. Energy 164, 339–354.
Wang, W., Mao, F., Du, L., Pan, Z., Gong, W., Fang, S., 2017. Deriving hourly PM2.5 concentrations from himawari-8 AODs over beijing-tianjin-hebei in China. Rem. Sens. 9, 858.
Wang, W., Mao, F., Pan, Z., Gong, W., Yoshida, M., Zou, B., Ma, H., 2019a. Evaluating aerosol optical depth from himawari-8 with sun photometer network. J. Geophys. Res.: Atmosphere 124, 5516–5538.
Wang, W., Mao, F., Zou, B., Guo, J., Wu, L., Pan, Z., Zang, L., 2019b. Two-stage model for estimating the spatiotemporal distribution of hourly PM1. 0 concentrations over central and east China. Sci. Total Environ. 675, 658–666.
Wei, J., Huang, W., Li, Z., Xue, W., Peng, Y., Sun, L., Cribb, M., 2019. Estimating 1-km-resolution PM2.5 concentrations across China using the space-time random forest approach. Rem. Sens. Environ. 231, 111221.

Yang, J., Cheng, Y., Du, L., Gong, W., Shi, S., Sun, J., Chen, B., 2019a. Analyzing the effect of the incidence angle on chlorophyll fluorescence intensity based on laser-induced fluorescence lidar. Optic Express 27, 12541–12550.
Yang, J., Du, L., Gong, W., Shi, S., Sun, J., Chen, B., 2019b. Analyzing the performance of the first-derivative fluorescence spectrum for estimating leaf nitrogen concentration. Optic Express 27, 3978–3990.
Yang, L.X., Wang, D.-c., Cheng, S.-h., Wang, Z., Zhou, Y., Zhou, X.-h., Wang, W.-x., 2007. Influence of meteorological conditions and particulate matter on visual range impairment in Jinan, China. Sci. Total Environ. 383, 164–173.
Yoo, J.M., Lee, Y.R., Kim, D., Jeong, M.J., Stockwell, W.R., Kundu, P.K., Oh, S.M., Shin, D.B., Lee, S.J., 2014. Corrigendum to "New indices for wet scavenging of air pollutants (O 3 ,CO, NO 2 , SO 2 , and PM 10) by summertime rain" [Atmos. Environ. Times 82 (2014), 226–237, 91, 226-237.
Yumimoto, K., Nagao, T.M., Kikuchi, M., Sekiyama, T.T., Murakami, H., Tanaka, T.Y., Ogi, A., Irie, H., Khatri, P., Okumura, H., 2016. Aerosol data assimilation using data from Himawari-8, a next-generation geostationary meteorological satellite. Geophys. Res. Lett. 43.
Yumimoto, K., Tanaka, T.Y., Yoshida, M., Kikuchi, M., Nagao, T.M., Murakami, H., Maki, T., 2018. Assimilation and forecasting experiment for heavy siberian wildfire smoke in may 2016 with himawari-8 aerosol optical thickness. J. Meteorol. Soc. Jpn. 96B, 133–149. Ser. II 96B.
Zhang, T., Gong, W., Wang, W., Ji, Y., Zhu, Z., Huang, Y., 2016. Ground level PM2.5 estimates over China using satellite-based geographically weighted regression (GWR) models are improved by including NO2 and enhanced vegetation index (EVI). Int. J. Environ. Res. Publ. Health 13, 1215.
Zhang, T., Zhu, Z., Gong, W., Zhu, Z., Sun, K., Wang, L., Huang, Y., Mao, F., Shen, H., Li, Z., Xu, K., 2018. Estimation of ultrahigh resolution PM2.5 concentrations in urban areas using 160 m Gaofen-1 AOD retrievals. Rem. Sens. Environ. 216, 91–104.
Zhang, Y., Ding, Z., Xiang, Q., Wang, W., Huang, L., Mao, F., 2019. Short-term Effects of Ambient PM1 and PM2.5 Air Pollution on Hospital Admission for Respiratory Diseases: Case-Crossover Evidence from Shenzhen, China. International Journal of Hygiene and Environmental Health, 113418.
Zhang, Y.L., Cao, F., 2015. Fine particulate matter (PM 2.5) in China at a city level. Sci. Rep. 5, 14884.
Zheng, S., Pozzer, A., Cao, C.X., Lelieveld, J., 2015. Long-term (2001–2012) concentrations of fine particulate matter ($PM_{2.5}$) and the impact on human health in Beijing, China. Atmos. Chem. Phys. 15, 5715–5725.